AIAA 2003-4473

# Vortex Thrust Chamber Testing and Analysis for O2-H2 Propulsion Applications

Martin J. Chiaverini, Matthew J. Malecki, Arthur Sauer
William H. Knuth, Daniel J. Gramer
Orbital Technologies Corporation (ORBITEC)
Madison, WI 53717

Joseph Majdalani
Advanced Theoretical Research Center
Marquette University
Milwaukee, WI 53233

**39th AIAA/ASME/SAE/ASEE Joint Propulsion Conference and Exhibit**
20–23 July 2003
Huntsville, AL

# Vortex Thrust Chamber Testing and Analysis for $O_2$-$H_2$ Propulsion Applications

Martin J. Chiaverini,* Matthew J. Malecki,† J. Arthur Sauer,‡ William H. Knuth,§ and Daniel J. Gramer¶
*Orbital Technologies Corporation, Madison, WI 53717*
and
Joseph Majdalani¥
*Marquette University, Milwaukee, WI 53233*

## ABSTRACT

A series of static thrust chamber firings were conducted with gaseous oxygen and hydrogen to investigate the specific impulse performance and thermal behavior of vortex combustion cold-wall chambers. Such thrust chambers employ an oxidizer swirl injector just upstream of the converging section of the nozzle to generate a coaxial, bi-directional vortex flow field in the combustion chamber. Depending on fuel injector design and chamber geometry, propellant mixing and combustion may be confined to the inner vortex, while the outer vortex protects the chamber wall from excessive heat loads. The results of the investigation indicated that while cold sidewall operation was achieved over a wide range of test conditions, faceplate heating rates were highly dependent on the chamber contraction ratio. Specific impulse efficiencies exceeding 97% were achieved. A statistical analysis indicated that both specific impulse efficiency and faceplate thermal behavior were strongly influenced by the fuel injector configuration. An approximate analytic model was developed to estimate the effect of chamber pressure on sidewall heating rates and indicated that the radiant heat flux from the reaction zone and the convective cooling from the outer vortex have approximately the same pressure-dependence.

## NOMENCLATURE

| | |
|---|---|
| $A$ | area |
| $AR$ | chamber aspect ratio (L/r) |
| $c_p$ | isobaric specific heat |
| $C^*$ | characteristic exit velocity |
| $CR$ | contraction ratio ($D_c^2/D^{*2}$) |
| $D$ | diameter |
| $D_h$ | hydraulic diameter |
| $D^*$ | nozzle throat diameter |
| $D_{conv}$ | throat convergence diameter |
| $ID$ | inner diameter |
| $I_{sp}$ | specific impulse |
| $L$ | length |
| $L^*$ | characteristic chamber length |
| $L/D$ | chamber length-to-diameter ratio |
| $M$ | momentum |
| $\dot{m}$ | mass flow rate |
| $O/F$ | oxidizer-to-fuel mass mixture ratio |
| $P$ | pressure |
| $\Delta P$ | pressure drop |
| $Pr$ | Prandtl number |
| $q$ | heat flux |
| $r$ | radius |
| $R$ | radius of curvature |
| $r^*$ | nozzle throat radius |
| $Re_D$ | Reynolds number based on diameter |
| $St$ | Stanton number |
| $T$ | temperature |
| $V$ | velocity |
| $X$ | mole fraction |
| $Z$ | axial coordiante |
| $\alpha$ | absorptivity |
| $\beta$ | GOX split ratio $\left[\dot{m}_{o,a}/\left(\dot{m}_{o,a}+\dot{m}_{o,sw}\right)\right]$ |
| $\varepsilon$ | emissivity |
| $\mu$ | viscosity |
| $\rho$ | density |
| $\sigma$ | Boltzmann constant (5.67e-8 $W/m^2K^4$) |

*Subscripts*

| | |
|---|---|
| $a$ | axial, auxiliary |
| $c$ | chamber, convective |
| $eff$ | efficiency |
| $fl$ | flame |
| $g$ | gas |
| $o$ | oxidizer, reference |
| $r$ | radiant |
| $s$ | surface |
| $sw$ | swirl |
| $tan$ | tangential |
| $th$ | throat |
| $tot$ | total |

* Principal Propulsion Engineer, Space Center, 1212 Fourier Drive. Member AIAA.
† Propulsion Scientist, Space Center, 1212 Fourier Drive. Member AIAA.
‡ Aerospace Engineer, Space Center, 1212 Fourier Drive. Member AIAA.
§ Chief Engineer, Space Center, 1212 Fourier Drive. Associate Fellow AIAA.
¶ Principal Aerospace Engineer, 1212 Fourier Drive. Member AIAA.
¥ Assistant Professor, Mechanical Engineering, 1515 W. Wisconsin Ave. Member AIAA.

## INTRODUCTION

THE thrust chamber cooling system represents a major consideration in the overall design of liquid propellant rocket engines. Common cooling methods include: regenerative cooling, film cooling, transpirational cooling, dump cooling, mixture ratio biasing, ablative cooling, and radiation cooling, as well as combinations of these methods. Regenerative cooling is often used for large- to medium-sized, high-pressure thrust chambers (such as the SSME and RL-10) and has the advantage of providing potentially high performance operation.[1] Kanda, et al., found analytically that regenerative cooling of a supersonic nozzle skirt resulted in better than a 1 s gain in specific impulse compared to an adiabatic engine. However, no change in $I_{sp}$ was noted for cooling subsonic components.[2] For high heat flux applications, regenerative cooling may require undesirably high coolant jacket pressure drops, which in turn lead to greater demands on the turbomachinery.[1] High-aspect-ratio cooling channels have been suggested as a means of reducing coolant pressure drop.[3] In addition, regenerative cooling can introduce very large thermal gradients in combustion chamber walls, accompanied by severe thermal stresses. The cyclic plastic deformation of the chamber wall that results from multiple firings can limit chamber lifetime.[4] Price and Masters investigated the use of liquid oxygen as a coolant for various high-pressure LOX/hydrocarbon thrust chambers. A portion of the investigation focused on examining the effect of an internal LOX leak on the structural integrity of the chamber wall. No metal burning or distress was observed, even after 22 engine cycles.[5]

Film-cooled chambers employ arrays of small holes to inject a cool liquid or gaseous boundary layer along the wall to reduce heat transfer rates. Film cooling introduces small performance losses due to the unburnt fuel, and is usually used to supplement regenerative cooling.[6] Schoenman has noted that low-thrust, liquid bipropellant engines may require significant amounts of film cooling, which degrades engine performance in favor of longer engine life.[7] According to both Rosenberg[8] and Schneider,[9] small spacecraft engines display significant performance improvements when film-cooling can be eliminated.

Transpirational cooling is similar to film cooling but uses a porous material rather than sets of discrete holes. Transpirational cooling has been used to cool injector faces in the SSME and J-2.[6] Porous material selection and construction methods may be limited by thermal stresses and mechanical stresses induced by the pressure differential between the coolant and combustion gases.[6]

In dump cooling systems, a small fraction of fuel from the main line is diverted to the chamber cooling passages, then expanded overboard. Dump cooling can be effective for hydrogen-fuel thrust chambers at low pressures, or for nozzle extensions.[10,11] Technical difficulties may include the design of the discharge nozzle and inadequate coolant flow rates.[1]

Biasing the mixture ratio of injectors on the periphery of the faceplate near the chamber sidewall to achieve lower-temperature combustion (usually fuel-rich) can be used to reduce chamber wall heat fluxes, but may cause losses similar to film-cooling.[1]

Ablative cooling system employ combustion chamber liners that pyrolyze when subject to a high heat flux and form a carbonaceous char layer that resists thermal, mechanical, and chemical attack. Similar to regenerative cooling, ablative cooling is often supplemented by film-cooling.[1] Ablative cooling is usually most suited to pressure-fed space engines operating at less than about 300 psia. However, a 650,000-$lb_f$ thrust, 700 psia ablative thrust chamber was recently tested.[12]

Radiation cooling is generally applicable to nozzle extensions due to high temperatures in the combustion chamber and throat, though use of pyrolytic graphite chambers and supplemental film cooling may extend the range of applications.[1] Gray has reported on a 20-N, radiation-cooled spacecraft thruster for attitude and orbit control.[13]

ORBITEC has recently investigated a new type of cooling method that can potentially offer additional benefits and design flexibility for various types of liquid propellant thrust chambers. The Vortex Combustion Cold-Wall (VCCW) chamber employs a coaxial, co-spinning, but bi-directional vortex flow field that can confine propellant mixing and burning to the core region of the chamber, alleviating heat transfer to the chamber surfaces. Figure 1 illustrates the overall concept. An oxidizer swirl injection ring is located between the chamber spool section and the nozzle, while fuel injection occurs at the head-end. (Though various fuel injection methods have been investigated, Figure 1 shows a generic injector for illustrative purposes.) Oxidizer injected through the swirl ring enters the chamber in a tangential manner, forming a vortex that spirals upwards along the chamber wall. The injected oxidizer is prevented from immediately flowing inward and out the nozzle by properly shaping the converging portion of the nozzle assembly and by the strong centrifugal forces associated with the tangential injection. At the faceplate, the outer vortex flows inward and forms a downward-spiraling inner vortex that exits the nozzle. Fuel is injected into the inner vortex where it is quickly vaporized and entrained by the swirling flow to ignite and burn with the oxidizer. Combustion is confined to the inner vortex and the flow field thus prevents the hot combustion products from contacting the chamber wall. In addition, the outer vortex can cool the wall to alleviate the effects of thermal radiation. Depending on the particular propellant combination and the fuel injection method, the fuel may be used to blanket the faceplate with a film-cooling layer, as in the current application with gaseous hydrogen. It should be noted that other cooling techniques, especially regenerative throat cooling and transpirational faceplate cooling, could be used in conjunction with the VCCW chamber. However, using vortex injection techniques should reduce the required coolant flow, decrease the overall turbopump pressure requirements, extend chamber lifetime by avoiding severe thermal stresses and cycling, and lower maintenance and operation costs.

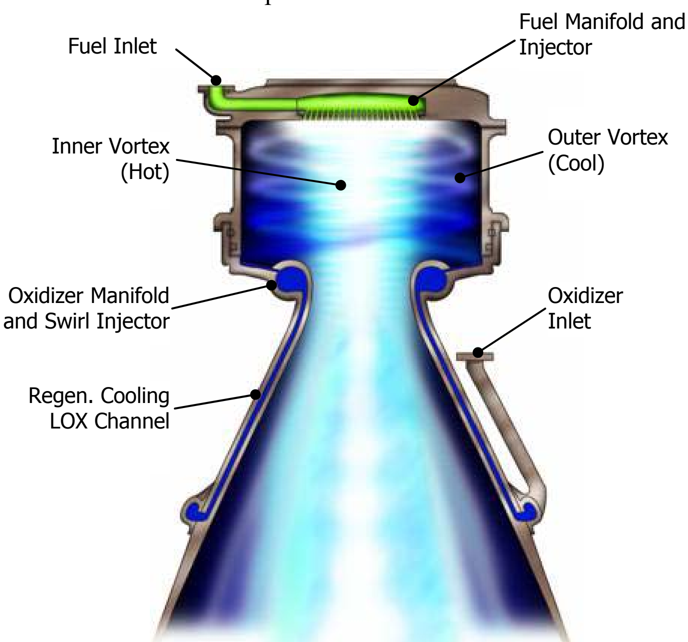


**Figure 1. Vortex Combustion Cold Wall Thrust Chamber (Artist's Concept)**

The basic features of the coaxial vortex flow field have previously been observed empirically[14] and analyzed both theoretically[15-17] and numerically[18,19] during recent investigations that parallel the current experimental effort. Figure 2 shows a video image of the lab-scale VCCW thrust chamber that was used to conduct initial hot-fire experiments discussed in Ref. [14]. This chamber sometimes employed a transparent acrylic test section for hot-firing flow visualization that was possible under particular test conditions due to the cold-wall operating characteristics. The photograph shows a side view image of a cylindrical combustion chamber burning GOX and $GH_2$ at a mixture ratio of 6 and a chamber pressure of about 135 psia. For scale, the outer diameter of the acrylic section is 3.5 inches. Notice that the combustion zone is confined to the inner region of the chamber by the coaxial flow field and that an annulus of non-combusting gas (primarily GOX) separates the chamber wall surface from the combustion zone.

The VCCW concept evolved from ORBITEC's prior work with vortex-injection hybrid rocket engines.[19,20] Figure 3a shows a numerically-simulated velocity field for a 500-$lb_f$ thrust vortex hybrid chamber. The CFD analysis was performed using the Finite Difference Navier Stokes (FDNS) code.[19] The fuel port shown in Fig. 3a has a length and inner diameter of 9 in. (23 cm) and 5.25 in. (13.4 cm), respectively. The GOX flow rate is 1.35 $lb_m$/s (0.615 kg/s). The tangential oxygen injector is located just above the entrance to the convergent section of the nozzle in Figure 3. Figure 3b shows the corresponding vector plot as predicted by a new, exact solution to the Navier Stokes equations recently developed by Vyas and Majdalani for non-reacting flow in vortex chambers.[15] Note the very favorable agreement between the computational and theoretical results. Both methods capture the main features of the coaxial, bi-directional vortex flow field discussed above for the VCCW: the flow enters the chamber tangentially above the nozzle, flows toward the head end, then flows inward, reverses direction, and flows toward the nozzle. Both the computational and theoretical solutions also indicate the existence of radial cross flow from the outer to the inner vortex along the length of the chamber. In addition, the existence of the so-called "mantle," the rotating but non-translating region separating the inner and outer vortices, is confirmed.

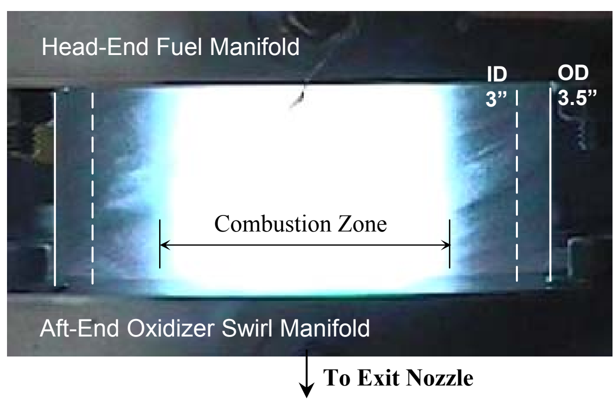


**Figure 2. Video Image of Lab-Scale VCCW Chamber Showing Combustion Zone Confined to Inner Vortex**

The work described here has been conducted under a NASA Phase II Small Business Innovation Research (SBIR) project to develop and test VCCW thrust chambers for oxygen-hydrogen propellants. In addition to the test programs, the project includes theoretical[15-17] and numerical[18] efforts to investigate vortex chamber flow field behavior for both hot-fire and cold-flow situations. Reference [21] discusses a related work that focuses on the use of particle imaging velocimetry (PIV) to measure velocity fields in a cold-flow vortex chamber. This article discusses the hot-fire testing efforts employed to characterize the performance and thermal behavior of two oxygen-hydrogen VCCW thrust chambers over a broad range of chamber configurations and operating conditions. The thrust chamber hardware and test methodology are first described. A discussion follows of the experimental results, including scoping tests, statistical testing, performance calculations, and thermal analysis. Finally, conclusions and areas of future work are discussed.

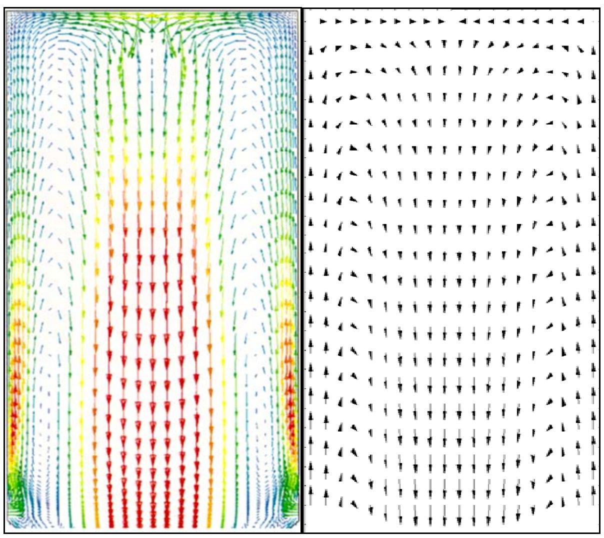

a) CFD b) Analytical

**Figure 3. Vector Plots Comparing CFD and Analytical Predictions for Coaxial Vortex Flow Field from Ref. [15]**

## METHOD OF APPROACH

The GOX/$GH_2$ hot-fire experiments were conducted using two thrust chamber assemblies. Figure 4 shows the VCCW-I, used to investigate a broad range of combustion chamber geometries and fuel injection methods. The VCCW-I was normally operated at a chamber pressure and thrust level of approximately 150 psia and 35 $lb_f$. However, several tests were conducted to examine chamber thermal behavior at higher pressure levels. The thrust chamber consists of modular hardware components to facilitate rapid variations in chamber configuration and was described in detail in Ref. [14]. Chamber inner diameters of 1, 1.25, 1.5, and 2 inches were tested. (Earlier testing also examined 2.5- and 3-inch chambers.[14]) In conjunction with the 0.5-inch throat, these chambers correspond to contraction ratios (chamber-to-throat area ratio) of 4, 6.25, 9, and 16. Additional test variables included chamber length, fuel injector style, faceplate contour, and converging nozzle section contour. All tests discussed here employed a flat faceplate. Reference [14] describes initial performance results obtained using a hemispherical faceplate. The exit nozzle had an area ratio of 2. In addition to the radial hydrogen injector shown in Fig. 4, showerhead, fuel-rich coaxial, and impinging swirl fuel injectors were also tested, but are not discussed here.

The results of a fuel injector characterization test effort appear in Ref. [14]. The propellant injectors were designed for nominal pressure drops of about 10% $P_c$. As discussed in Ref. [14], an auxiliary axial GOX injector in the faceplate, aligned with the chamber longitudinal axis, was used to enhance combustion in the core vortex. VCCW-I instrumentation included pressure transducers, thermocouples, and a load cell for thrust measurement. A spark igniter was employed to ignite the main propellants in the combustion chamber.

Figure 5 shows a schematic assembly of the VCCW-II, which accommodated higher-pressure testing up to approximately 500 psia, corresponding to a thrust of about 250 $lb_f$. Similar to the lab-scale VCCW-I, the VCCW-II had a modular design to provide flexibility in chamber length, faceplate geometry, and propellant injector design. Though the VCCW-II can accommodate spool sections of various inner diameter, all tests reported here utilized 2-inch ID combustion chambers. The 0.66-in. throat diameter provided a contraction ratio of 9.2. The exit nozzle had an area ratio of 5.

Test variables for the VCCW-II program included chamber length, swirl GOX injector pressure drop, auxiliary GOX injector pressure drop, radial $GH_2$ injector pressure drop, number of hydrogen injection ports, and auxiliary GOX flow rate (defined as a fraction of total GOX flow). Various propellant injectors were fabricated to allow for independent control of flow rate and pressure drop for GOX swirl and auxiliary GOX injection, and for independent control of pressure drop and number of injectors for $GH_2$ injection. Neither the faceplate nor the exit nozzle contour were varied during the VCCW-II test matrix discussed here. Instrumentation included pressure transducers, thermocouples for faceplate, sidewall, and nozzle temperature measurements, and a load cell for thrust measurement. A spark igniter was used to achieve main propellant ignition.

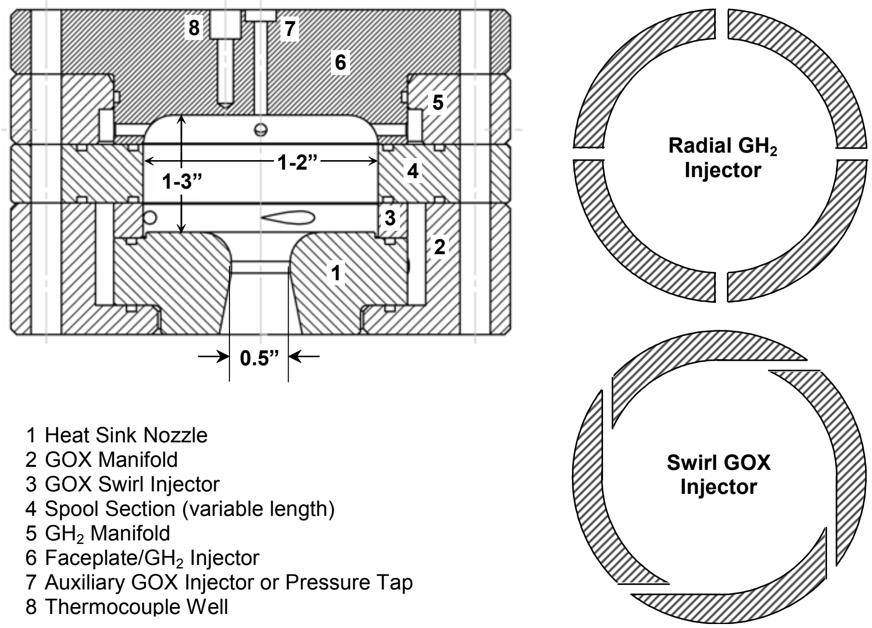


**Figure 4. VCCW-I Thrust Chamber Assembly**

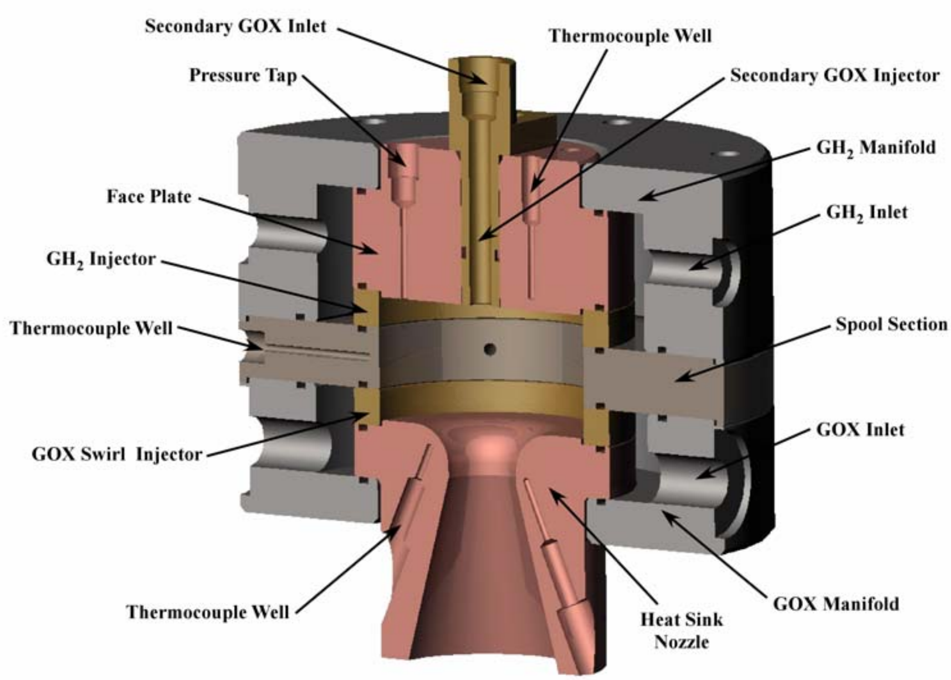


**Figure 5. VCCW-II Thrust Chamber Assembly**

The specific impulse efficiency was used as the primary measure of thrust chamber performance. This $I_{sp,eff}$ was calculated by comparing the experimentally determined specific impulse at ambient conditions to the theoretical equilibrium ambient specific impulse based on calculations using the CEA code developed at NASA/GRC.[22] An averaging procedure was used over the steady-state portion of the thrust and propellant line pressure profiles to determine thrust and flow rates used in the calculations. Reference [14] presents the details of this performance evaluation method. It should be noted that this type of chemical equilibrium analysis probably results in a somewhat conservative estimate of the thrust chamber performance because it does not account for real nozzle effects such as boundary layer losses, non-axial flow, and finite-rate chemistry, which probably result in losses of a few percent.[6] Reference [14] also discusses the results of an analysis to estimate the effects of swirl flow on the specific impulse performance. For typical hot-firings, it was found that the residual swirl velocity in the exit nozzle flow had a very small effect on the resulting specific impulse – less than the estimated experimental error of +/- 2% on the $I_{sp}$ calculation. For a practical VCCW-based propulsion system, the calculated effect of swirl flow on delivered $I_{sp}$ was entirely negligible.[14] The residual swirl velocity component in the exit nozzle flow will also impart some amount of torque to the host vehicle. However, we do not anticipate that this effect is particularly large given the relatively modest swirl strengths required to generate the coaxial velocity field.[14] In addition, a portion of the angular momentum resulting from swirl oxidizer injection will dissipate due to viscous interactions in the thrust chamber prior to reaching the nozzle exit plane. Characterizing the nozzle exit plane angular momentum distribution, resulting residual torque, and specific impulse represents a goal of the computational fluid dynamics effort.[18]

The efficiency of the characteristic exit velocity, $C^*_{eff}$, was not employed as a primary performance metric because the vortex flow field present in the combustion chamber generates radial pressure gradients that complicate the determination of an average chamber pressure for calculating experimental $C^*$ values. An analysis similar to that discussed above for the $I_{sp}$ efficiency was conducted for a limited number of tests that had well-characterized radial pressure gradients for calculating the average chamber pressure. (The full head-end pressure transducer array was not available for all chamber configurations due to the particular fuel injector and faceplate geometry.) The results of the analysis indicated $C^*$ efficiencies of about 94 to 99% for the tests that also demonstrated high $I_{sp,eff}$.

## RESULTS AND DISCUSSION

Several series of hot firings were conducted to characterize the performance and thermal behavior of both the VCCW-I and VCCW-II thrust chambers. Gaseous oxygen and gaseous hydrogen were used in all cases. Based on the results presented in Ref. [14], the radial injector was used as the baseline configuration for both the VCCW-I and VCCW-II test series described here. The VCCW-I experiments focused on examining the effects of chamber L*, contraction ratio, length-to-diameter ratio, and exit nozzle contour on performance and thermal behavior. These experiments served to focus the statistical test matrix conducted with the VCCW-II, which examined the effects of chamber length, injector pressure drops, and GOX split ratio (β) on specific impulse and chamber thermal characteristics.

### Thrust Chamber Performance

Figure 6 shows a typical thrust and chamber pressure history from the VCCW-I test program. Main propellant ignition occurs at t=1 s and results in a small pressure and thrust spike. The GOX and $GH_2$ propellants reach their full flow rate at t=2.5 s and were shut off at 6.5 s. At this time, a low-pressure nitrogen flow was activated to purge the propellant lines and chamber. Note that both the pressure and thrust plots indicates stable combustion with no pressure oscillations. Such results were typical for both the VCCW-I and VCCW-II thrust chamber test series.

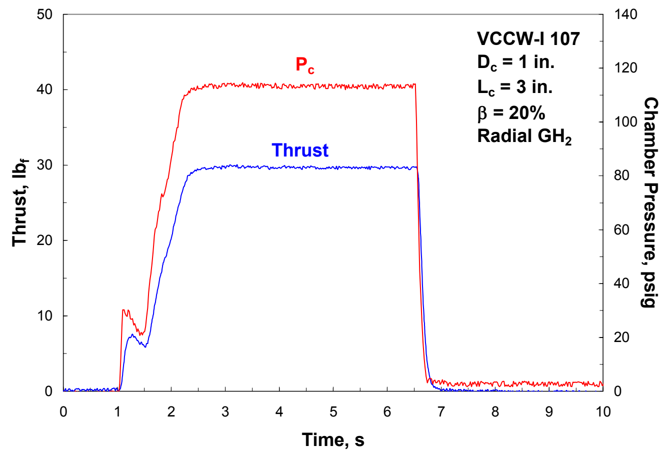


**Figure 6. Typical Thrust and Chamber Pressure Profiles for VCCW-I Hot-Fire Tests**

<u>VCCW-I Scoping Test Results</u>

Figure 7 summarizes the VCCW-I specific impulse efficiency results as a function of chamber $L^*$ for various chamber contraction ratios (CR) ratios. The chamber length-to-diameter ratio also varies, though the particular values do not appear in Figure 7. The chamber contraction ratio was varied by selecting specific values of 1, 1.25, 1.5, 2, 2.5, and 3 in. for the chamber inner diameter. When combined with the exit nozzle throat diameter of 0.5 in., contraction ratios of 4, 6.25, 9, 16, 25, and 36 result from these diameter values. Chamber $L^*$ variations within a given CR group correspond to different chamber lengths, where the length is defined as the distance between the inner surface of the faceplate and the base of the GOX swirl injector. All tests shown in Figure 7 employed the radial fuel injection method, propellant injectors designed for nominal pressure drops of 10% $P_c$ (15 psid), a mixture ratio of 6, and a GOX split ratio (β) of approximately 20%. This value of β led to optimum performance during early testing[14] and was adopted here as the nominal value for the VCCW-I testing.

Figure 7 illustrates several important results of the VCCW-I test series. First, high performance of about

97% specific impulse efficiency was achieved, even at the relatively low chamber pressure of 150 psia characteristic of the VCCW-I testing. In addition, except for the 1-inch diameter chamber (CR=4), performance appeared to improve somewhat at lower $L^*$ values. This effect may result from injecting the hydrogen and oxygen in closer proximity as the chamber size is decreased, thus improving propellant mixing. It is interesting to note that the 1-inch chamber tests (CR=4) had an $L^*$ of about 12 in., while the 1.5-inch chamber tests (CR=9) spanned a range of 9 to 27 in. However, even at an $L^*$ of 9 in., the 1.5-inch chamber displayed a significantly higher performance level of about 96% than the 1-inch chamber (about 82% $I_{sp,eff}$) at a larger $L^*$ of 12 in.

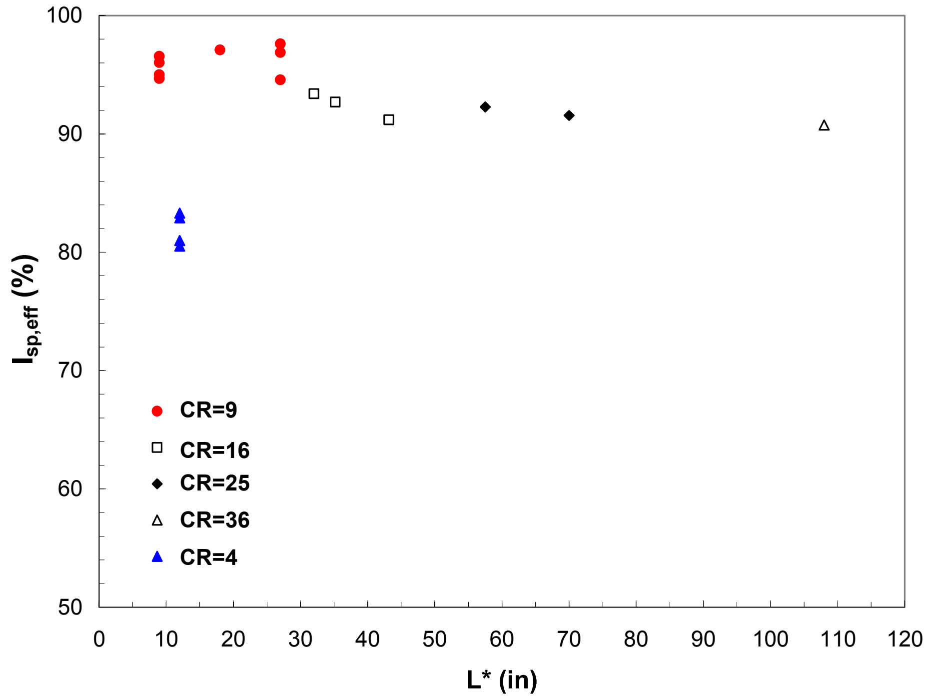


**Figure 7. Variation of Specific Impulse Efficiency with $L^*$ and CR for VCCW-I at Nominal Test Conditions (GOX and $GH_2$, O/F=6, $\beta$=20%, Nozzle C, $T_{theo}$=35 $lb_f$, $P_{c,theo}$=150 psia)**

We theorize that the relatively low performance associated with the 1-inch diameter chamber (CR=4) arises from one of two effects, or possibly a combination of both: the close radial proximity of the GOX swirl jets to the converging portion of the exit nozzle and an extended L/D chamber. First, the close radial proximity of the GOX swirl injector to the converging portion of the exit nozzle may allow a portion of the gaseous oxygen to flow out the nozzle rather than toward the faceplate, thereby bypassing the majority of the reaction zone. As shown in Figure 4, the converging portion of the exit nozzle has a 0.25-inch radius of curvature, and the throat has a radius of 0.25 in. Therefore, for the 1-inch diameter assembly (0.5-inch chamber radius), the GOX swirl ports enter the chamber at the same radial location where the nozzle plate begins to converge to the throat. For this configuration, there is no flat, annular base area below the injectors to force the outer vortex up the wall toward the faceplate. Therefore, the swirling GOX may flow toward the throat without mixing with the $GH_2$ at the head-end, leading to poor performance. On the other hand, the 1.5-inch and 2-inch chambers have annular regions 0.25 and 0.5 in. wide, respectively, between the swirl port inlets and the start of the converging contour. Figure 8 compares sections views of three VCCW-I configurations, showing the relative proximity of the GOX swirl ports to the nozzle converging section for the different chamber diameters.

The nozzle throat temperature histories provide evidence for this behavior. As shown in Figure 9, the high-performance tests, using the 1.5- and 2-inch chamber, generally indicated nozzle throat temperatures rises of about 500 to 600 $^oC$ after about 5 s of steady-state operation whereas the corresponding tests with the 1-inch chamber indicated a maximum temperature of less than 100 $^oC$. This finding suggests that a layer of cool oxygen, escaping along the nozzle, acts as a film coolant for the throat. Employing a different nozzle plate contour with an adequately sized annular base below the swirl GOX jets could allow for high performance with smaller contraction ratio chambers. This situation would potentially prove advantageous for minimizing the overall heat load to the combustion chamber by reducing the cross sectional area of the faceplate, which is generally subject to higher temperatures than the sidewalls.

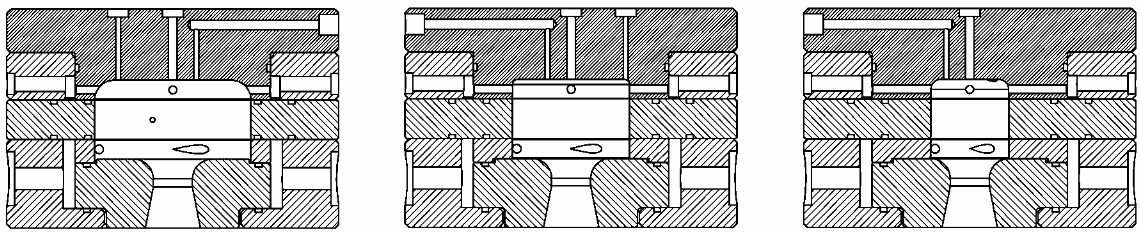

a) CR=16 (2” ID) b) CR=9 (1.5” ID) c) CR=4 (1” ID)

**Figure 8. Section Views of Three VCCW-I Configurations**

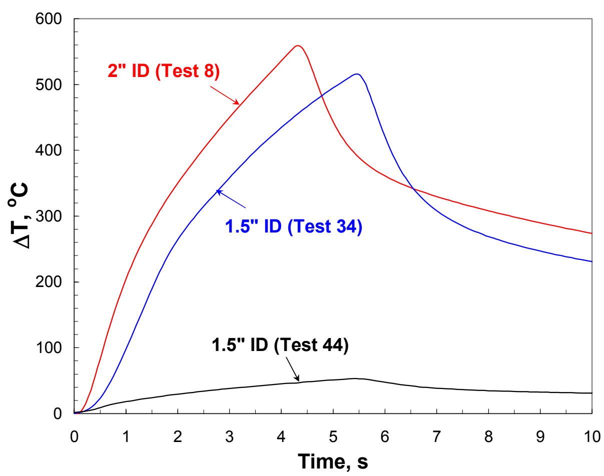


**Figure 9. Nozzle Throat Temperatures**

In addition to the exit nozzle contour, the lower performance of the 1-inch configuration may be associated with chamber length-to-diameter (L/D) effects. The 1-inch chamber had an L/D of 3, whereas the 1.5- and 2-inch chambers had L/D values of 0.67 to 2 for the tests shown in Figure 7. For a given chamber diameter, longer chambers necessarily have larger axial distance between the GOX swirl injector and radial $GH_2$ injector. This separation may somewhat inhibit propellant mixing in the faceplate region, leading to lower performance than for shorter L/D chambers.

The recent work by Vyas, Majdalani, and Chiaverini[15] supports this hypothesis. Though derived for non-reacting vortex flow in a circular cylinder, their results are believed to be qualitatively accurate for the present work. Figure 10 shows sample results for the streamlines in representative vortex chambers of various aspect ratios (AR, the ratio of chamber length to chamber radius, effectively twice the L/D). Note that the streamlines are symmetric about the chamber axis, represented by the r=0 line. Chambers with relatively low aspect ratios (10a) have streamlines more concentrated at the faceplate than large aspect-ratio chambers (10c). This situation would tend to favor more intense mixing and combustion near the faceplate fuel injectors for relatively short chambers. In addition, the theoretical analysis also mathematically quantifies that *the coaxial vortex flowfield has a maximum swirl intensity at the faceplate.*[15] Therefore, the VCCW should benefit from fuel injection and propellant mixing in the faceplate region. This result suggests that optimum performance may arise from a chamber geometry that allows for maximum oxygen transport to the faceplate region, but with adequate downstream chamber volume to complete the propellant reaction.

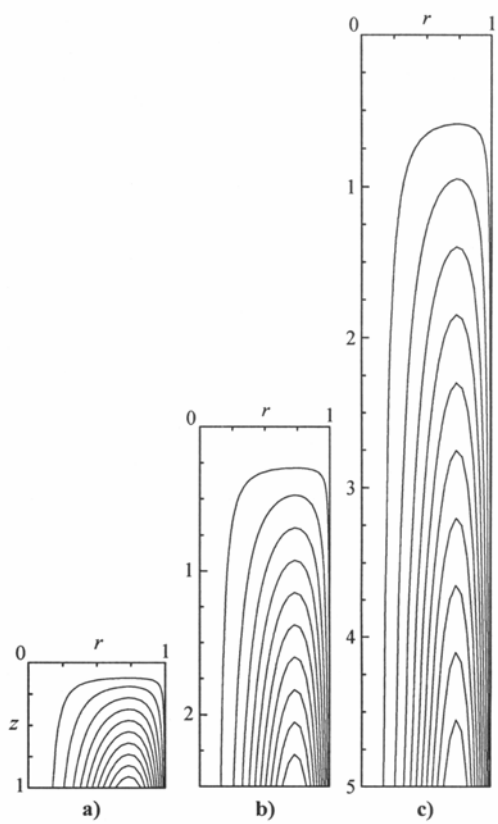


**Figure 10. Analytical, Non-Reacting Streamline Patterns at Different Aspect Ratios: a) 1 (L/D=0.5), b) 3 (L/D=1.5), and c) 5 (L/D=2.5) from Ref. [15]**

In order to investigate the effects discussed above for vortex chambers with relatively large L/D and/or small CR, a second VCCW-I test series was conducted with additional thrust chamber hardware to investigate how the contour of the converging section of the nozzle and the chamber L/D affected performance. This test series included a set of 1.25-inch chamber components, as well as additional exit nozzles with various converging geometries. The 1.25-inch components were designed to provide various L/D values between 0.8 and 3.2.

All exit nozzles had a throat diameter of 0.5 in., a diverging cone angle (full angle) of 22.4 degrees, and an exit area ratio of 2. However, the designs had various converging radii of curvature so that the width of the flat annular region below the GOX swirl jets could be varied by selecting different nozzles for a given chamber diameter. A geometric parameter called the nozzle convergence diameter, $D_{conv}$, which equals the throat diameter plus twice the radius of curvature, was defined to characterize the salient relationship between the nozzle contour and the chamber diameter. As shown in Figure 11, this parameter corresponds to the radial location along the nozzle top surface where convergence toward the throat begins.

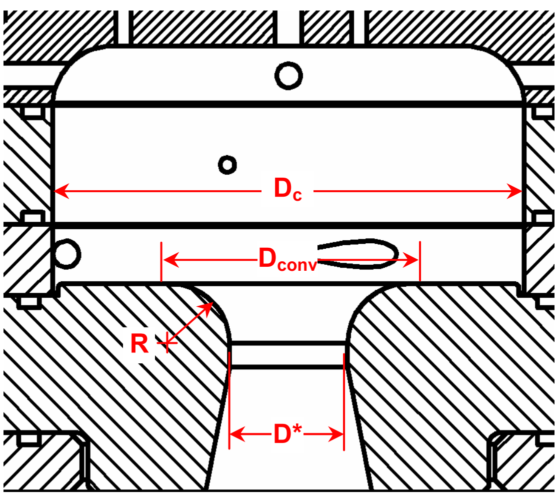


**Figure 11. Geometric Nozzle Parameters**

Table 1 shows the values of $D_{conv}$ for each nozzle/chamber diameter combination as a percentage of chamber diameter. Note that a $D_{conv}$ value of 100% in Table 1 represents a nozzle/chamber combination with no annular base beneath the swirl jets, and is exemplified by the 1-inch chamber and nominal (C) nozzle. Note further that nozzles A and B had $D_{conv}$ values that exceeded the 1-inch chamber diameter, while nozzle A exceeded the 1.25-inch chamber diameter. These combinations were not tested.

Figures 12 and 13 summarize the results of this test series. It is evident from Figure 12 that varying the converging nozzle contour had no significant effect on specific impulse efficiency for any of the four chambers tested, and therefore did not increase the performance of the 1-inch chamber. However, Figure 13 indicates that the combustion chamber length-to-diameter does appear to effect $I_{sp,eff}$. Notice that the data for the 1.25-inch chamber (CR=6.25) indicates a trend of decreasing performance with increasing L/D for L/D values larger than about 2. For the longest chamber (L/D=3.2), the $I_{sp,eff}$ has an average value of about 87%, indicating a 7% drop from the value at the shortest chamber (L/D=0.8). This result suggests that reducing the length of the 1-inch chamber could potentially improve performance. The relatively low performance of the 1-inch chamber (CR=4) and high performance of the 1.5-inch chamber (CR=9) in Figures 12 and 13 serves to reinforce that the chamber contraction ratio also plays a role in performance, at least above some threshold value for a given set of chamber operating conditions. It should also be noted that, while not investigated here, performance of low contraction ratio or long L/D chambers may benefit from higher injection swirl velocity.

**Table 1. Values of Nozzle Convergence Diameter for Various Nozzle/Chamber Combinations**

| | Dc=1” | Dc=1.25” | Dc=1.5” | Dc=2” |
|---|---|---|---|---|
| **Nozzle A** | -- | -- | 88.9% | 66.7% |
| **Nozzle B** | -- | 93.3% | 77.8% | 58.3% |
| **Nozzle C** | 100.0% | 80.0% | 66.7% | 50.0% |
| **Nozzle D** | 83.4% | 66.7% | 55.6% | 41.7% |
| **Nozzle E** | 66.7% | 53.3% | 44.4% | 33.3% |

An area of current work focuses on developing empirical correlations to describe the VCCW thrust chamber performance as a function of geometric variables, such as L/D and CR, as well as propellant injection variables, such as swirl GOX momentum. These efforts will be reported in a future article. Here, it is worth mentioning that Vyas and Majdalani have recently developed a dimensionless parameter called the vortex Reynolds number that may prove beneficial for predicting the experimental results.[16]

<u>VCCW-II Statistical Test Results</u>

The VCCW-I test program focused primarily on characterizing the performance and thermal behavior of various vortex thrust chamber configurations as a function of geometric parameters (CR, L/D, $L^*$, $D_{conv}$) without detailed consideration of the propellant injection parameters. The VCCW-II test series discussed here focused on propellant injection variables, as well as the effect of chamber length. All VCCW-II tests employed a contraction ratio of 9.2 (2-in. chamber, 0.66-in. throat) and oxidizer-to-fuel mixture ratio of approximately 6/1.

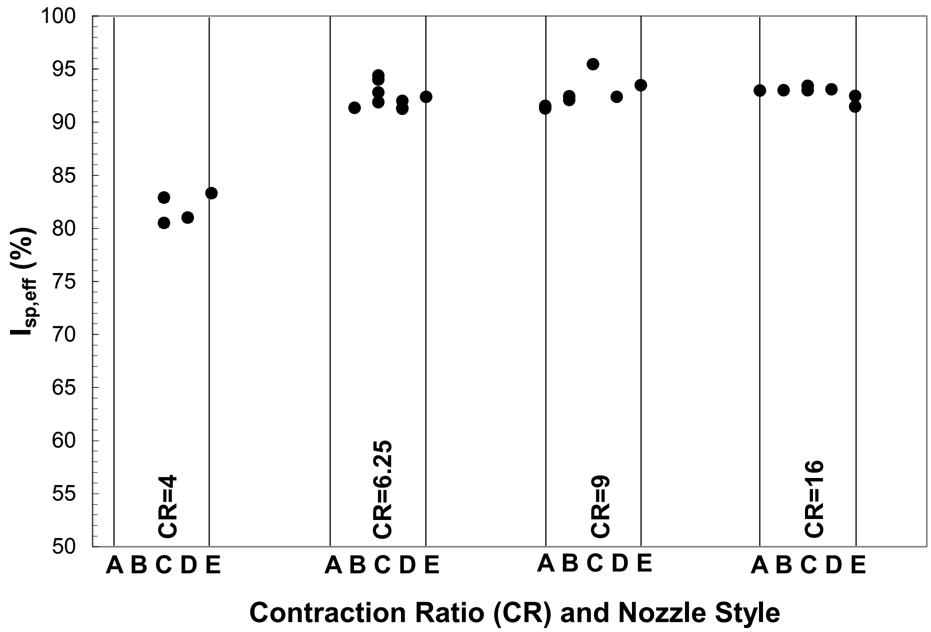


**Figure 12. Variation of Specific Impulse Efficiency with CR and Nozzle (data points correspond to L/D ≤ 2, except for CR=4 where L/D=3)**

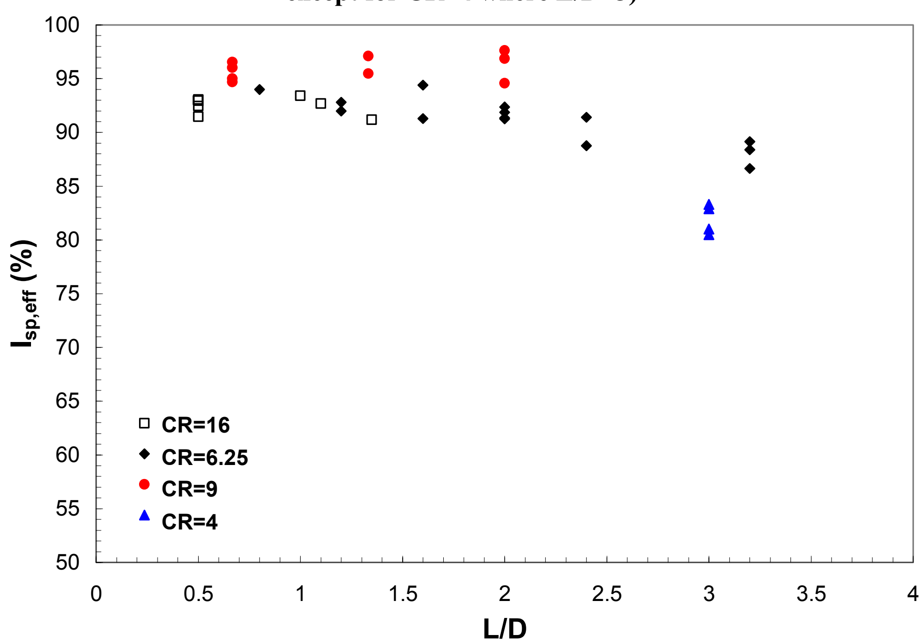


**Figure 13. Variation of Specific Impulse Efficiency with CR and L/D**

Table 2 shows the screening matrix used to determine the sensitivity of specific impulse efficiency and sidewall and faceplate heating rates to chamber length, propellant injector pressure drops (in $\%P_c$), GOX split ratio ($\beta$, in % total GOX flow rate), and number of ports in the $GH_2$ radial injector. The specific impulse results are discussed here and the thermal behavior in later sections.

The screening matrix was designed using statistical analysis software to determine the main effects of test variables on performance and thermal behavior. Analysis of the resulting data assumed that second and higher order interaction effects are not present in the system. The goals of the statistical screening analysis are to provide a general understanding of thrust chamber operation and identify which variables have the most influence on performance. Though these results should be considered somewhat preliminary due to the sparseness of the screening matrix, they are useful for indicating general trends and guiding future tests to more thoroughly examine the effects of the statistically significant variables.

**Table 2. VCCW-II Statistical Screening Test Matrix ($\Delta P$ in $\%P_c$, $\beta$ in % total GOX flow rate)**

| Run No. | $L_c$ (in) | $\beta$ | Swirl GOX $\Delta P$ | Aux. GOX $\Delta P$ | $GH_2$ $\Delta P$ | No. $GH_2$ Ports |
|---|---|---|---|---|---|---|
| 1 | 2 | 40 | 20 | 10 | 20 | 4 |
| 2 | 2 | 20 | 10 | 10 | 10 | 8 |
| 3 | 1 | 40 | 20 | 10 | 10 | 8 |
| 4 | 1 | 20 | 10 | 10 | 20 | 4 |
| 5 | 1 | 40 | 10 | 20 | 20 | 8 |
| 6 | 1 | 20 | 20 | 20 | 10 | 4 |
| 7 | 2 | 40 | 10 | 20 | 10 | 4 |
| 8 | 2 | 20 | 20 | 20 | 20 | 8 |

Various swirl and auxiliary GOX injectors were designed to provide for independent control of the oxygen pressure drops and flow rate schedule (to achieve the two values of $\beta$) required by Table 2. The *total* GOX flow rate did not vary appreciably. Similarly, four $GH_2$ injectors allowed independent control of injection pressure drop and number of ports. The test matrix was conducted using propellant flow schedules consistent with theoretical chamber pressures of 250 psia (approximate theoretical sea-level thrusts of 125 $lb_f$), and a mixture ratio of 6. Additional testing was also conducted at 400 and 500 psia levels.

The VCCW-II screening matrix indicated a maximum $I_{sp,eff}$ of 96.6% for Run No. 1 in Table 2. The lowest specific impulse efficiency of 85.5% occurred for Run No. 5. Figure 14 illustrates the results of a sensitivity analysis for specific impulse efficiency, and indicates that the number of $GH_2$ injection ports had the most significant effect, followed closely by both the swirl and secondary GOX injector pressure drops. The $GH_2$ injector pressure drop and the chamber length also affected $I_{sp,eff}$,, but to a lesser extent. However, the GOX split ratio had no discernible effect, possibly because the selected values of 20% and 40% are beyond a threshold level where performance is greatly affected by variations in $\beta$.

Figure 15 shows the $I_{sp,eff}$ response surfaces vs. the six test variables. Note that for the two-level screening matrix (Table 2) the response surfaces are flat, indicating linear variations in $I_{sp,eff}$. For the ranges of the variables examined in Table 2, Figure 15 indicates the following trends toward higher specific impulse performance: fewer $GH_2$ ports, higher swirl GOX injector pressure drop, lower auxiliary GOX injector pressure drop, lower $GH_2$ injector pressure drop, and longer chamber length. These results seem to indicate that larger fuel jets provide higher performance, a result which may appear counterintuitive. However, larger radial $GH_2$ jets may penetrate more effectively into the core vortex to burn with the secondary GOX. Higher swirl GOX injection pressure drops probably enhances mixing, leading to higher combustion efficiency. However, slower auxiliary GOX injection may enhance combustion in the core vortex by allowing for longer residence times. Finally, longer chambers provide larger $L^*$ to complete combustion before entering the nozzle. (It should be noted that the screening matrix used L/D ratios of 0.5 and 1; therefore the performance decrease noted from VCCW-I testing for relatively long L/D chambers probably did not arise.)

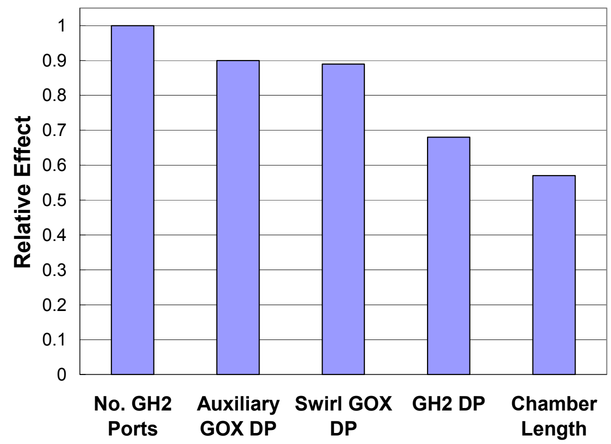


**Figure 14. Sensitivity of $I_{sp,eff}$ to VCCW-II Screening Matrix Test Variables**

The VCCW-I and VCCW-II results suggest that the performance of the vortex combustion chamber is governed by several competing effects. For a given inner diameter (effectively, the CR), longer chambers have relatively greater L* and length-to-diameter ratio. Chambers with longer characteristic length provide more time for propellant mixing and combustion to proceed toward completion. However, the corresponding larger L/D may cause a lower percentage of the swirl-injected GOX to reach the faceplate region and instead flow into the core vortex at axial stations downstream of the faceplate. Therefore, it appears that for a given set of operating conditions and chamber diameter, an optimum chamber length exists. Above this length, L/D effects may decrease swirl oxidizer transport to the fuel surface, which tends to reduce performance. Below this length, the L* is inadequate to provide complete combustion.

Similarly, chambers with a given throat size may have an optimum chamber diameter that provides vigorous mixing and associate high performance. At diameters larger than optimal, viscous dissipation in the outer vortex may adversely affect propellant mixing near the faceplate. At diameters smaller than optimal, the radial inflow velocity may be large enough to inhibit a significant portion of oxygen flow toward the head end.

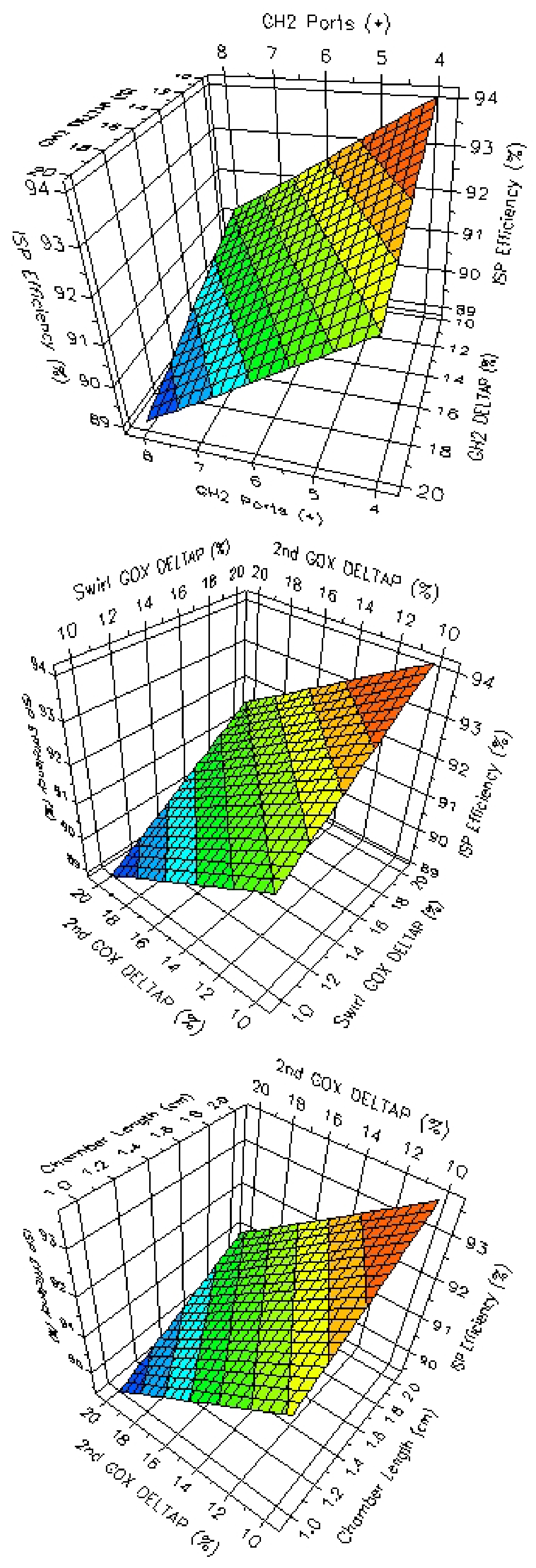


**Figure 15. Response of $I_{sp,eff}$ to Screening Matrix Test Variables**

## Thrust Chamber Thermal Behavior

The VCCW-I and VCCW-II were also used to characterize thermal behavior of vortex combustion chamber. Figure 16 shows typical faceplate temperature profiles at three radial stations: 0.3, 0.5, and 0.7 in. from the center of the faceplate. Main propellant ignition occurs at t=0 and shutdown occurs at t=5.5 s. These plots clearly indicate higher temperatures near the center of the faceplate than near the chamber wall. The inner thermocouple indicates a temperature rise of about 430 $^{o}$C, while the outermost thermocouple indicated a temperature increase of about 230 $^{o}$C. In addition, the relatively long time delay (approx. 3 s) between chamber shut down and peak temperature at r=0.7 in. indicates that the outer region of the faceplate is probably subject to radial conduction from the central region rather than direct heating from the combustion zone. Since the central region of the faceplate is apparently subject to the most intense heat load, the innermost thermocouple measurement at r=0.3 in. was used as the primary metric for characterizing faceplate heating behavior for the VCCW-I.

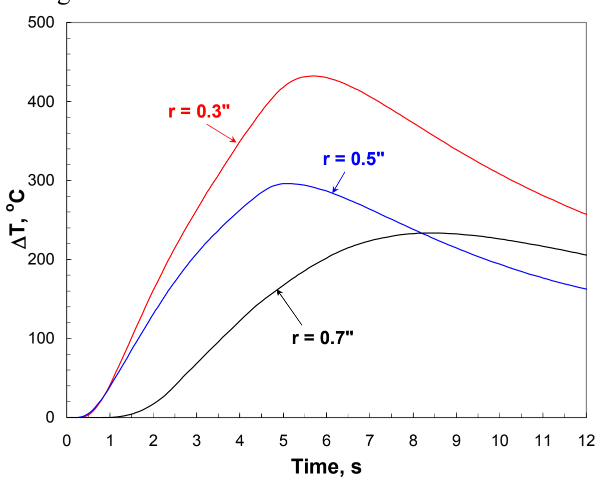


**Figure 16. Faceplate Temperature Profiles at Various Radii for 2-inch Diameter VCCW-I Chamber**

Figure 17 shows the faceplate temperature behavior (at r=0.3 in.) for several VCCW-I chamber configurations defined by chamber diameter and chamber length. All tests employed a radial fuel injector just below the faceplate, as shown in Figure 4. All tests were conducted at a mixture ratio of approximately 6 and a GOX split ratio of 20%. Except for the 400 psia test, propellant flow rates corresponded to a theoretical thrust and chamber pressure of 35 $lb_f$ and 150 psia, respectively. The chamber contraction ratio clearly has a very significant effect on the faceplate heating behavior. The 2-inch diameter, 2-inch long chamber undergoes a temperature rise of about 430 C during the test, nearly 3 times larger than that of the 1.5-inch chamber. This difference may be explained by a smaller faceplate area exposed to the reaction zone and relatively more effective cooling ability of the hydrogen jets in closer proximity to the center of the faceplate. Thus, the fuel jets do not need to penetrate across as large a region before entering the core vortex, thereby more effectively blanketing the faceplate.

It is interesting to note that increasing the chamber pressure by increasing the propellant flow rates (with a fixed exit nozzle throat size of 0.5 inch) did increase the faceplate heating rate, but not to the same extent as increasing the chamber diameter. The higher chamber pressure leads to a larger convective heat transfer rates in accordance with higher gas density, as well as an increase in the radiant heat flux. However, these effects are partially offset by the increased film cooling that corresponds to higher fuel flow rates across the faceplate.

The sidewall heating rates and temperature profiles were typically lower than the corresponding faceplate heating rates, as shown in Figure 18. As discussed in Ref. [14], the sidewall heating rates decreased as the chamber volume decreased, with chamber diameter having a stronger effect than chamber length. Test 8, with a 2-inch diameter chamber, had an average heating rate of about 12 $^{o}$C/s during the test, while Test 42, with a 1.5-inch chamber, had a heating rate of about $^{o}$7 C/s. More effective wall cooling may result from smaller chamber surface area to be cooled, as well as a relatively higher angular velocity of fluid in the outer vortex as chamber diameter is decreased for a given GOX tangential injection velocity. Higher angular velocity implies a larger number of revolutions per unit length of chamber wall as the outer vortex spirals toward the faceplate. This phenomena may improve the wall cooling effect.

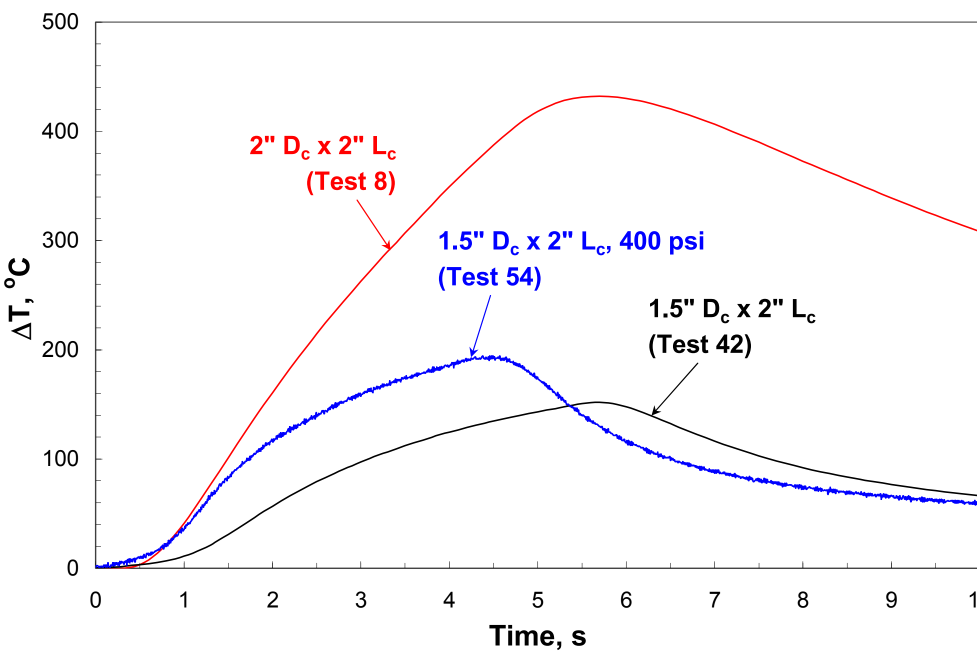


**Figure 17. Faceplate Temperature Rise Profiles at r=0.3 in. for Various Chamber Diameters (All Tests at 150 psia Except Test 54 at 400 psia)**

A comparison of Tests 29 and 54 in Figure 18 indicates the relative effect of chamber pressure on the sidewall heating rates. Though the same thrust chamber was used for both tests (1.5 in. ID, 2 in. length, 0.5 in. throat) Test 54 was conducted at a 400 psi level by using elevated propellant flow rates, as compared to the 150 psi chamber pressure for Test. 29. However, the tests had very similar sidewall temperature profiles, with total temperature increases of less than 40 $^{o}$C during the 5 s test time. This finding suggests that while radiant heat flux to the chamber surfaces increases with chamber pressure, the convective cooling of the outer vortex also increases due to the higher oxygen flow rate required to achieve the higher chamber pressure for a fixed throat size (in this case, 0.5 in.). Both tests also appear to approach a steady-state sidewall temperature during the 5.5 s test.

Based on these results, the question arises as to whether increasing the chamber pressure by increasing the propellant flow rates (for a fixed chamber geometry) tends to favor the radiant heat flux to the chamber wall surface or the convective cooling effect of the outer vortex. An analysis based on semi-empirical correlations from the literature was therefore conducted to estimate the relative magnitude of thermal radiation and convection on the chamber sidewalls as a function of pressure. No attempt has been made to develop a comprehensive thermal model of the thrust chamber which includes ignition transients, subsurface conduction from the un-cooled regions of the chamber (such as the nozzle and throat regions) to the sidewalls, etc.

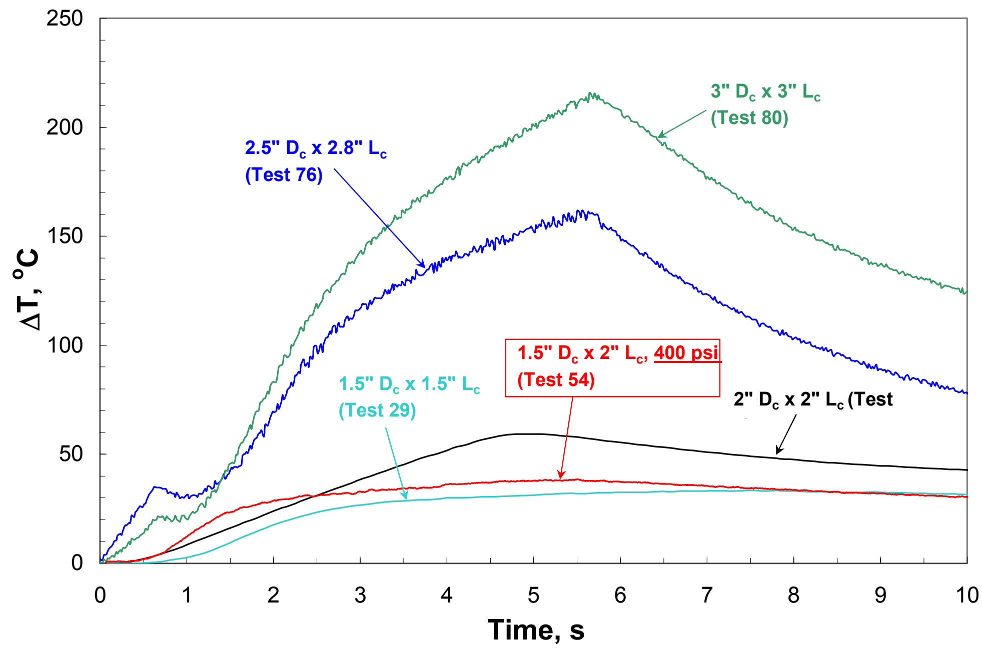


**Figure 18. Sidewall Temperature Rise Profiles for Various Chamber Configurations (All Tests at 150 psia Except Test 54 at 400 psia)**

The radiant heat flux depends on many parameters, including the chamber pressure, propellant mixture ratio (mole fraction of $H_2O$), characteristic reaction zone thickness, emissivity of the chamber wall surface, and the geometry of the chamber and reaction zone. A simplified model has been initiated to examine the effects of chamber pressure, $O_2$-$H_2$ mass mixture ratio, and reaction zone thickness on reaction zone emissivity and radiant heat flux. In the vortex combustion chamber, the reaction zone is believed to reside in the inner vortex while the outer vortex of cool GOX separates the reaction zone from the chamber walls. However, $O_2$ (as well as $H_2$) is a diatomic, non-polar gas that does not emit radiation and is essentially transparent to incoming radiation, and thus can be ignored in the present formulation. Water vapor, on the other hand, is a polar molecule that emits and absorbs strongly over a wide temperature range, and is thus the primary combustion product of interest for determining radiant heat flux behavior.[23] Ignoring the effects of the endwalls (faceplate and nozzle base) on the overall radiation exchange in the chamber, the net radiation exchanged between the reaction zone and the chamber sidewall may be written as:[23]

$$q_r = \sigma\varepsilon_s\left(\varepsilon_g T_g^{4} - \alpha_g T_s^{4}\right) \quad (1)$$

For the current situation of interest, the second term in parentheses, which represents the radiant heat flux from the chamber surface to the reaction zone, may be ignored due to the (expected) large temperature difference between the flame and wall. Assuming that the reaction zone has a temperature of approximately 3500 K, the wall temperature would have to be on the order of 1000 K to make even a 1% difference in $q_{rad}$.

The $H_2O$ gas phase emissivity may be estimated using Leckner's method, as presented by Modest.[24] Leckner's correlations calculate a reference emissivity at atmospheric pressure, given by

$$\varepsilon_o\left(p_a, p = 1\ bar, T_g\right) = exp\left[\sum_{i=0}^{m}\sum_{j=0}^{n} c_{ji}\left(\frac{T}{T_o}\right)^{j}\left(log_{10}\frac{p_aL}{(p_aL)_o}\right)^{i}\right] \quad (2)$$

where the reference temperature, $T_O$, equals 1000 K and $(p_aL)_O$ equals 1 bar cm. For pressure conditions other than atmospheric, a new emissivity based on the reference emissivity of Eq. (2) is calculated:

$$\frac{\varepsilon\left(p_aL, p, T_g\right)}{\varepsilon_o\left(p_aL, 1\cdot bar, T_g\right)} = 1 - \frac{(a-1)(1-P_E)}{a+b-1+P_E}exp\left(-c\left[log_{10}\frac{(p_aL)_m}{p_aL}\right]^{2}\right) \quad (3)$$

where the effective pressure, $P_E$, depends on the total pressure, partial pressure of the gas component under consideration, and non-dimensional temperature $T/T_o$. Table 3 gives Leckner's correlation parameters appearing in Eqs. (2) and (3) for water vapor.[24]

**Table 3. Leckner's Correlation Constants for $H_2O$**

| Parameter | Value |
|---|---|
| m, n | 2, 2 |
| $c_{00}, c_{10}, c_{20}$<br>$c_{01}, c_{11}, c_{21}$<br>$c_{02}, c_{12}, c_{22}$ | –2.2118, –1.1987, 0.035596<br>0.85667, 0.93048, –0.14391<br>–0.10838, –0.17156, 0.045915 |
| $P_E$ | $\dfrac{\left(p + 2.56 p_a / \sqrt{t}\right)}{p_o}$ |
| $(p_aL)_m/(p_aL)_o$ | $13.2t^2$ |
| a | 2.479, t < 0.75<br>1.888 – 2.053 $\log_{10}t$, t > 0.75 |
| b | $1.10 / t^{1.4}$ |
| c | 0.50 |
| $T_o$ = 1000 K, $p_o$ = 1 bar, t = $T/T_o$, $(p_aL)_o$ = 1 bar–cm | |

In order to investigate the radiant heat flux behavior, the chamber pressure and effective flame thickness, L, were treated as parameters. A chemical equilibrium code was used to calculate the theoretical flame temperature and $H_2O$ mole fraction ($X_{H2O}$) corresponding to the combustion of $O_2$-$H_2$ at the selected pressure and a mixture ratio of 6 (see Figure 19).

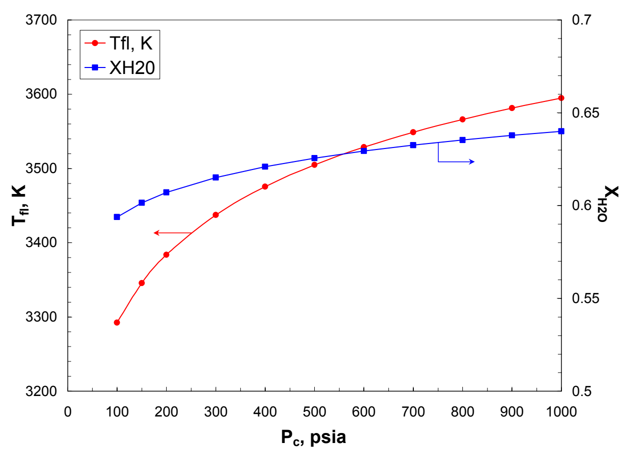


**Figure 19. Chemical Equilibrium Calculations for $O_2$-$H_2$ Combustion at O/F=6**

For the simplified approach followed here, it was assumed that the reaction zone, of thickness $L_{fl}$, had a uniform flame temperature and water vapor concentration. Though the reaction zone thickness is difficult to accurately estimate, a representative value of 1 in. was used here. This value corresponds roughly to the diameter of the inner vortex for a 1.5-inch chamber, based on the analytic results of Ref. [15], and allows the determination of relative trends with chamber pressure. It is worth mentioning that current efforts focus on use of a laser diagnostic system to interrogate the reaction zone in a transparent vortex chamber. This investigation should help characterize the properties of the reaction zone in the inner vortex.

For convective heating and cooling in tubes subject to swirling flow from a tangential injector, but in the absence of combustion, Dhir[25] found experimentally that:

$$\frac{St_{sw}}{St_o} = 1 + 1.93\left(\frac{M_{tan}}{M_{tot}}\right)^{0.6} Pr^{-1/7} \exp\left[-m\left(\frac{z}{D_h}\right)^{0.6}\right] \tag{4}$$

where

$$m = 0.89\left(\frac{M_{tan}}{M_{tot}}\right)^{0.2} Re_D^{-0.18}\, Pr^{-0.083} \tag{5}$$

The term $M_{tan}/M_{tot}$ represents the ratio of tangential to total axial momentum in the port. According to Dhir,[25] this parameter is equivalent to the ratio of port-to-injector areas ($A_p/A_{inj}$) for the current situation, and therefore does not vary with pressure for a thrust chamber of given geometry.

The term $St_{sw}/St_o$ accounts for the enhanced local heat transfer due to tangential injection. Using the definition of St

$$St = \frac{q_c}{\rho V c_p \left(T_s - T_\infty\right)} \tag{6}$$

and the reference $St_o$ for fully-developed pipe flow

$$St_o = 0.023\,\mathrm{Re}_D^{-0.2}\,\mathrm{Pr}^{-0.7} \tag{7}$$

the convective (cooling) heat flux can be calculated by combining Eqs. (4), (6), and (7):

$$q_c = \frac{St_{sw}}{St_o}\left(0.023\,\mathrm{Re}_D^{-0.2}\,\mathrm{Pr}^{-0.7}\right)\left[\rho V c_p \left(T_s - T_\infty\right)\right] \tag{8}$$

For a given thrust chamber geometry burning a given propellant combination, the chamber pressure can be varied by changing the propellant flow rates into the combustion chamber. (Modifying the exit nozzle throat size will also affect the chamber pressure, but is not consistent with either the test methodology employed during this investigation, nor the assumption of fixed chamber geometry.) For the vortex combustion cold-wall thrust chamber configuration, the swirl oxidizer flow rate controls the convective cooling rate on the chamber sidewall. In order to determine the relative trend in convective cooling that accompanies a change in chamber pressure via propellant flow rate variations (and therefore, thrust), it is necessary to recast various terms in Eq. (8) as functions of swirl GOX flow rate. First, the Reynolds number for internal flow may be calculated from

$$\mathrm{Re}_D = \frac{\dot{m}_o D_H}{A_{ref}\,\mu} \qquad (9)$$

since the mass velocity may be written as

$$\rho V = \frac{\dot{m}_o}{A_{ref}} \qquad (10)$$

Substituting Eqs. (9) and (10) into Eq. (8) yields

$$q_c = \frac{St_{sw}}{St_o}\left[0.023\left(\frac{D_H}{\mu}\right)^{-0.2}\frac{1}{A_{ref}^{0.8}}\mathrm{Pr}^{-0.7}\right]\left[c_p\left(T_s - T_\infty\right)\right]\dot{m}_o^{0.8} \qquad (11)$$

Though the ratio of Stanton numbers in Eq. (11) does depend on $\mathrm{Re}_D$, as shown explicitly in Eq. (5), the dependency is weak: $St_{sw}/St_o$ increases only about 10% over an order of magnitude change in $\mathrm{Re}_D$. Therefore, for the current approximate analysis, this weak dependence is ignored, leading to a conservative approach for the convective cooling since $St_{sw}/St_o$ increases for greater Reynolds numbers.

The geometric parameters in Eq. (11) do not vary with pressure or thrust. However, the appropriate reference area and hydraulic diameter in Eq. (11) correspond to those of the outer vortex, which controls the convective cooling. According to the results of the analytic model, the outer vortex occupies an annular region from the sidewall in to a diameter equivalent to 71% of the chamber diameter.[15] In addition, the size of the outer vortex does not vary with chamber pressure,[15] therefore, $D_H$ and $A_{ref}$ may be considered constants. In addition, the viscosity, specific heat, and Prandtl number of the injected oxygen are assumed constant with respect to pressure and flow rate. Finally, we make the *a priori* assumption that the temperature differential between the injected GOX and the sidewall remains approximately constant, then check this assumption for consistency with the empirical results (e.g., Figure 18). Based on these considerations, we find that convective heat flux varies with swirl oxidizer mass flow to the 0.8 power:

$$q_c \propto \dot{m}_o^{0.8} \qquad (12)$$

Figure 20 illustrates the results of the analysis for both radiant and convective heat transfer trends, and the water vapor emissivity. Note that both the relative radiant heat flux and relative convective cooling increase at nearly the same rate with respect to increasing pressure. A best-fit curve to the calculations indicates that $q_r/q_{r,o}$ varies with pressure to the 0.82 power.

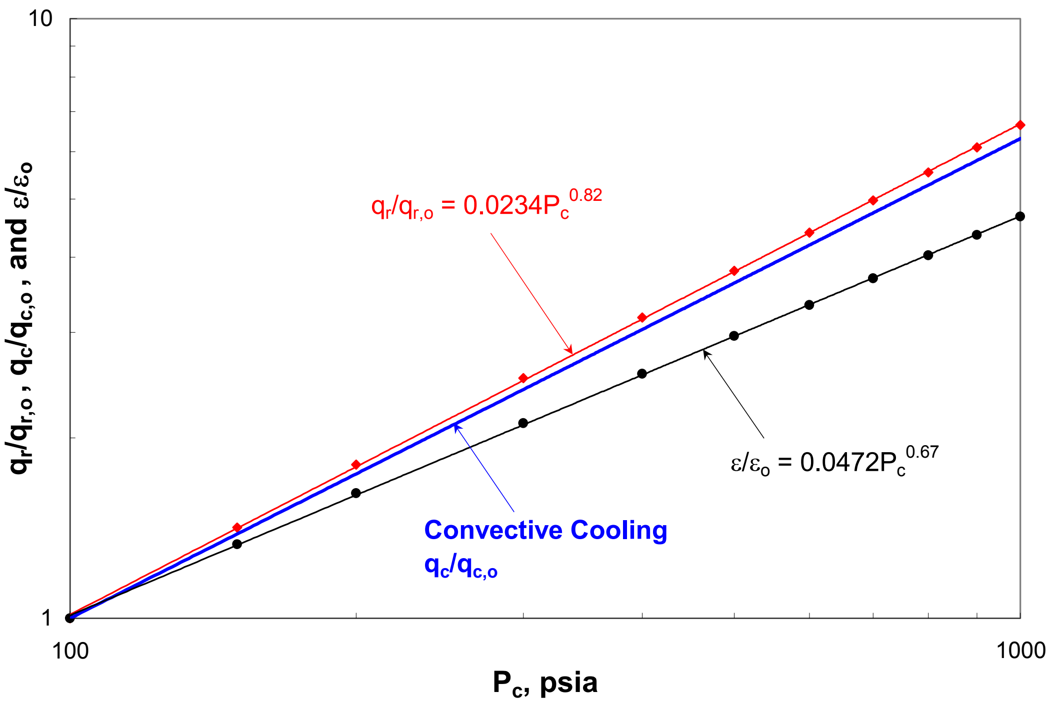


**Figure 20. Sidewall Heat Transfer Analysis Showing Trends of Radiant Heat Flux and Convective Cooling with Chamber Pressure**

The relative emissivity of $H_2O$ has a smaller pressure dependence than the radiant heat flux due to the additional effect of flame temperature on $q_r$. Though the flame temperature does not depend strongly on $P_c$, as shown in Figure 19, the radiant heat flux has a strong dependency on temperature ($T^4$), such that even small changes in flame temperature may affect $q_r$ significantly.

The results of the approximate heat transfer analysis appear to agree qualitatively with the experimental results shown in Figure 18, suggesting that sidewall temperature may not vary greatly with chamber pressure due to the similar pressure-dependency of radiant heat flux and convective cooling for a given thrust chamber.

A statistical analysis similar to that of the specific impulse performance was also conducted for the faceplate heating behavior for the VCCW-II screening test matrix shown in Table 2. As for the VCCW-I testing, the thermocouple nearest the center of the faceplate consistently recorded the highest temperature change and was therefore used as the reference measurement for faceplate heating behavior. Run No. 7 in Table 2 provided the lowest faceplate heating rate, while the highest occurred for Run No. 3.

Figure 21 indicates that the number of injection ports in the $GH_2$ had the most significant effect faceplate heating, while the GOX split ratio β had no discernible effect, as for the $I_{sp,eff}$ results. Statistical analysis indicated the following trends toward lower heating rates: fewer $GH_2$ ports, lower swirl GOX injector pressure drop, higher auxiliary GOX injector pressure drop, lower $GH_2$ injector pressure drop, and longer chamber length.

Though preliminary due to the sparseness of the test matrix, these results seem to indicate that larger, slower fuel jets provide better faceplate cooling. Fewer, larger jets (with higher individual momentum than a larger number of smaller jets) may penetrate further across the faceplate before complete entrainment into the vortex flow field, while slower jets may spread out and blanket the faceplate more completely prior to entrainment into the main flow. In addition, faceplate heating appears to increase as oxygen transport and swirl momentum, which should enhance propellant mixing, are increased near the faceplate. Both higher GOX swirl velocity (larger pressure drop) and shorter chamber lengths favor more intense GOX swirl at the faceplate, while lower-velocity auxiliary injection may create a wider GOX jet that has a longer residence time in the faceplate region. It is interesting to note that a combination of large swirl GOX injector pressure drop and low auxiliary GOX injector pressure drop led to both high specific impulse efficiency and high faceplate heating rate. This result again suggests that vigorous combustion in the faceplate region results in high combustion efficiency.

All measured sidewall temperature rises for the VCCW-II screening matrix were quite similar to those of the VCCW-I testing shown in Figure 18, and did not display much dependence on the test variables. Therefore, a sensitivity analysis was not conducted. This general result is in qualitative agreement with the VCCW-I testing which indicated that chamber contraction ratio had the greatest effect on faceplate temperature. However, the VCCW-II testing did not consider CR as a test variable.

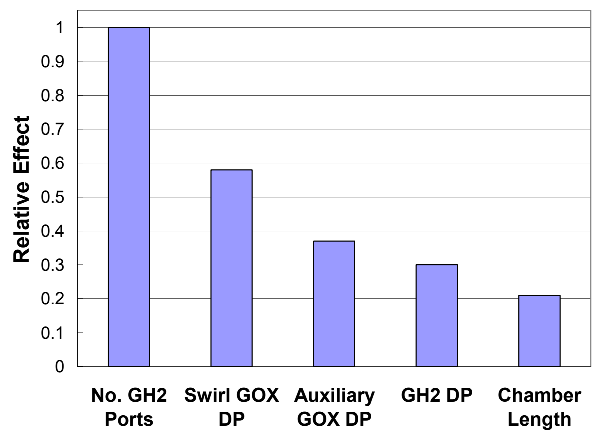


**Figure 21. Sensitivity of $T_{face}$ to VCCW-II Screening Matrix Test Variables**

## SUMMARY AND CONCLUSIONS

The main purpose of this work was to further the development of vortex combustion thrust chambers for liquid propellant rocket engine applications. A modular, lab-scale thrust chamber assembly (VCCW-I) was tested to determine the effects of combustion chamber and nozzle geometry on specific impulse performance and chamber thermal behavior. A second test program was conducted with a larger thrust chamber (VCCW-II) to obtain initial data on performance and thermal characteristics as a function of injection parameters. Major results of the investigation include:

- Specific impulse efficiency of about of 97% was obtained in both vortex combustion thrust chambers
- Chamber geometry testing indicated that performance tended to decrease somewhat for length-to-diameter ratios in excess of about 2
- Performance also decreased for contraction ratios below 6, and seemed to peak at contraction ratios of about 6 to 9
- Statistical analysis of the screening matrix indicated that performance depended relatively strongly on

the fuel injector configuration and the swirl and auxiliary GOX pressure drops, with high swirl and low auxiliary pressure drops leading to high performance

- Faceplate temperatures displayed a significant dependence on chamber diameter and fuel injector configuration, with narrower chambers an larger fuel jets leading to lower heating rates
- Sidewall temperatures also depended strongly on chamber diameter, though very low sidewall heating rates, on the order of 7 $^{o}$C/s at 400 psi, were obtained in conjunction with high specific impulse efficiencies (upper 90%s)
- Chamber sidewall heating rates did not display a significant dependence on chamber pressure, apparently due to the similar effects of elevated pressure on both thermal radiation (acting to heat the wall) and convective cooling from the outer vortex
- No significant pressure oscillations or combustion instabilities were observed or measured.

Future work on this program will include additional testing with the VCCW-II thrust chamber assembly to more thoroughly examine the effects of chamber geometry, injector characteristics, and faceplate contour on specific impulse and heating rates, testing of an alternate thrust chamber using liquid oxygen and gaseous hydrogen, and additional data analysis to more fully characterize performance and thermal characteristics of vortex combustion cold-wall thrust chambers.

## ACKNOWLEDGEMENT

This work was performed under a NASA Phase II SBIR project, contract no. NAS8-02020. The support and encouragement of Mr. Huu Trinh, NASA Marshall Space Flight Center's Technical Monitor, is gratefully acknowledged. The authors also thank Mr. Brant White, Mr. Christopher St.Clair, Dr. Eric Rice, and Mr. Ronald Teeter of Orbital Technologies Corporation for their assistance in conducting this work.

## REFERENCES

1. Huzel, D.K., and Huang, D.H., *Modern Engineering for Design of Liquid-Propellant Rocket Engines*, AIAA Progress in Aeronautics and Astronautics, Vol. 147, 1992, pp. 84-104, 381-382.
2. Kanda, T., Masuya, G., Wakamatsu, Y., Kanmuri, A., Chinzei, N., Niino, M., "Effect of Regenerative Cooling on Rocket Engine Specific Impulse," *AIAA Journal of Propulsion and Power* Vol. 10, No. 2, 1994, pp. 286-288.
3. Wadel, M.F., and Meyer, M.L., "Validation of High Aspect Ratio Cooling in a 89 kN (20,000 $lb_f$) Thrust Combustion Chamber," AIAA Paper 96-2584, 32nd Joint Propulsion Conference, Lake Buena Vista, FL, July 1996, also NASA-TM-107270.
4. Riccius, J.R., "Stationary and Dynamic Thermal Analyses of Cryogenic Liquid Rocket Combustion Chamber Walls," AIAA Paper 2002-3694, 38th Joint Propulsion Conference, Indianapolis, IN, July 2002.
5. Price, H.G., and Masters, P.A., "Liquid Oxygen Cooling of High Pressure LOX/Hydrocarbon Rocket Thrust Chambers," NASA-TM-88805, August 1986.
6. Sutton, G.P., *Rocket Propulsion Elements*, 6th ed., John Wiley & Sons, New York, 1992, pp. 72-73, 90, 109-116, 282, 289-294.
7. Schoenman, L., "4000 F Materials for Low Thrust Rocket Engines," AIAA Paper 93-2406, 1993.
8. Rosenberg, S.D., and Schoenman, L., "A New Generation of High Performance Engines for Spacecraft Propulsion," AIAA Paper 91-2039, 27th Joint Propulsion Conference, Sacramento, CA, June 1991.
9. Schneider, S.J., "High Temperature Thruster Technology for Spacecraft Propulsion," IAF-91-254, also NASA-TM-105348.
10. Haggander, J., Stenholm, T., Boman, A., Lang, Y., "Design and Manufacturing of Advanced Nozzle Demonstrator for Vulcain Mk II," AIAA Paper 95-2538, 31st Joint Propulsion Conference, San Diego, CA, July 1995.
11. Anantha, K., Tucker, K., "CFD Analysis of the STME Nozzle Flowfield," NASA Goddard Space Flight Center Tenth Workshop for Computational Fluid Dynamic Applications in Rocket Engines, Part 2, pp. 831-847.
12. Gavitt, K., and Mueller, T., "Testing of the 650 $Klb_f$ $LOX/LH_2$ Low Cost Pintle Engine (LCPE)," AIAA Paper 2001-3987, 37th Joint Propulsion Conference, Salt Lake City, UT, July 2001.
13. Gray, H.L, "Design and Development of the UK 20N Bipropellant Thruster," AIAA Paper 90-2053, 26th Joint Propulsion Conference, Orlando, FL, July 1990.
14. Chiaverini, M.J., Malecki, M.M., Sauer, J.A., and Knuth, W.H., "Vortex Combustion Chamber Development For Future Liquid Rocket Engine

Applications," AIAA Paper 2002-4149, 38th Joint Propulsion Conference, Indianapolis, IN, July 2002.

15. Vyas, A.B., Majdalani, J., and Chiaverini, M.J., "The Bidirectional Vortex: Part 1 – An Exact Inviscid Solution," AIAA Paper 2003-5052, 39th Joint Propulsion Conference, Huntsville, AL, July 2003.

16. Vyas, A.B., Majdalani, J., and Chiaverini, M.J., "The Bidirectional Vortex: Part 2 – A Viscous Core Solution," AIAA Paper 2003-5053, 39th Joint Propulsion Conference, Huntsville, AL, July 2003.

17. Vyas, A.B., Majdalani, J., and Chiaverini, M.J., "The Bidirectional Vortex: Part 3 – Multiple Solutions," AIAA Paper 2003-5054, 39th Joint Propulsion Conference, Huntsville, AL, July 2003.

18. Fang, D.Q., Majdalani, J., and Chiaverini, M.J., "Simulation Of The Cold-Wall Swirl-Driven Combustion Chamber," AIAA Paper 2003-5054, 39th Joint Propulsion Conference, Huntsville, AL, July 2003.

19. Knuth, W.H., Gramer, D.J., Chiaverini, M.J., Sauer, J.A., Whitesides, R. H., and Dill, R. A., "Preliminary CFD Analysis of the Vortex Hybrid Rocket Chamber and Nozzle Flow Field," AIAA Paper 98-3351, 34th Joint Propulsion Conference, Cleveland, OH, July 1998.

20. Knuth, W.K., Chiaverini, M.J., Sauer, J.A., and Gramer, D.J., "Solid-Fuel Regression Rate Behavior of Vortex Hybrid Rocket Engines," *AIAA Journal of Propulsion and Power* Vol. 18, No. 3, 2002, pp. 600-609.

21. Anderson, M., Valenzuela, R., Rom, C., Bonazza, R., and Chiaverini, M.J., "Vortex Chamber Flow Field Characterization for Gelled Propellant Combustor Applications," AIAA Paper 2003-4474, 39th Joint Propulsion Conference, Huntsville, AL, July 2003.

22. McBride, B. J., and Gordon, S., *Computer Program for Calculation of Complex Chemical Equilibrium Compositions and Applications*, NASA Reference Publication 1311, NASA John H. Glenn Research Center at Lewis Field, Cleveland, OH, June 1996.

23. Incropera, F.P., and De Witt, D.P., *Fundamentals of Heat and Mass Transfer*, 3rd ed., John Wiley & Sons, 1990, pp. 827-833.

24. Modest, Michael F., *Radiative Heat Transfer*, McGraw-Hill, Inc., New York, 1993, pp. 362-371.

25. Dhir, V.K., and Chang, F., "Heat Transfer Enhancement Using Tangential Injection," *ASHRAE Transactions*, Vol. 98, Part 2, pp. 383-390, 1992.